Quantum oscillations of Kondo screening phases in strong magnetic fields

Po-Hao Chou,[1] Chung-Hou Chung,[3] and Chung-Yu Mou[1,2,4]

[1]*Physics Division, National Center for Theoretical Sciences, Taipei 10617, Taiwan, Republic of China*

[2]*Center for Quantum Technology and Department of Physics, National Tsing Hua University, Hsinchu, Taiwan 300, Republic of China*

[3]*Electrophysics Department, National Yang Ming Chiao Tung University, Hsinchu, Taiwan 300, Republic of China*

[4]*Institute of Physics, Academia Sinica, Nankang, Taiwan, Republic of China*

(Received 8 February 2022; revised 25 October 2022; accepted 26 October 2022; published 3 November 2022; corrected 28 November 2022)

We generalize the iterative diagonalization procedure adopted in the method of numerical renormalization group to analyze the Kondo effect in strong magnetic fields, where the density of states for itinerary electrons at the chemical potential varies discontinuously as the magnetic field changes. We first examine phases of many-body ground states in the presence of a single impurity. By investigating the change of the z component of total spin, ΔS_z, and spin-spin correlation between the impurity and conduction electrons, we find that there are three states competing for the ground state when Zeeman splitting is present. One of the states is a doublet in which the impurity spin is unscreened. The other two states are Kondo screening states with $\Delta S_z = \frac{1}{2}$ and 1, in which the impurity spin is partially screened and completely screened, respectively. For Kondo systems with two impurities in strong magnetic fields, we find that the interplay between the Kondo screening effect, Rudermann-Kittel-Kasuya-Yoshida interaction, and quantum oscillations due to Landau levels determines the ground state of the system. A combination of these three factors results in different screening scenarios for different phases in which spins of two impurities can form spin-0 or spin-1 states, while impurity spins in these phases can be either screened, partially screened, or unscreened by conduction electrons. The emergence of the ground state from these competing states oscillates with the change of magnetic field, chemical potential or inter-impurity distance. This leads to quantum oscillations in magnetization and conductivity. In particular, we find extra peak structures in longitudinal conductivity that reflect changes of Kondo screening phases and are important features to be observed in experiments. Our results provide a complete characterization of phases for Kondo effect in strong magnetic fields.

DOI: 10.1103/PhysRevB.106.195107

I. INTRODUCTION

How the magnetic order emerges from the interaction between localized magnetic moments and itinerary electrons is an important issue to understand magnetism in correlated metals. The issue has been clarified at the level of single magnetic moment, in which the moment gets screened and results in a correlated Kondo screening state [1,2]. It is further realized that when the number of magnetic moments exceeds one, the Rudermann-Kittel-Kasuya-Yoshida (RKKY) interaction is induced between moments, which starts to compete with the Kondo effect. Depending on the distance between moments, the induced coupling between two magnetic moments oscillates between ferromagnetic (FM) or antiferromagnetic (AFM) coupling, leading to complicated competitions among correlated singlet states, triplet states, and Kondo screening states [3–11].

While the above understandings have been known for a while, they were based on the analysis in conventional metallic systems in which the density of states (DOS) for itinerary electrons is nearly a constant near the chemical potential μ. When external magnetic fields are present, the assumption of constant DOS breaks down. In the case when magnetic fields are weak, the degeneracy at the chemical potential for different spin components is lifted. This leads to the differentiation of possible correlated states for two impurities and makes these correlated states observable in experiments [12]. More recently, the de Haas–Van Alphen effect is observed for Kondo insulators in strong magnetic fields [13–15]. The oscillation is shown to result from the emergence of Landau levels in electronic structures [16]. In this case, the density of states for itinerary electrons at the chemical potential varies discontinuously as the magnetic field changes. Consequently, the Kondo screening effect should be entirely different. For instance, when μ lies at the middle between two Landau levels without particle-hole symmetry, as suggested by Kondo effects studied for gapped systems (such as semiconductors) [17–19], one expects that the system should undergo a quantum phase transition from singlet to doublet if the spacing between Landau levels is compared with the Kondo temperature, leading to the breakdown of screening effect at low temperature. Here the energy gap in the gapped system plays a similar role as the spacing of Landau levels for Kondo systems in strong magnetic fields. In addition, the Kondo effect is shown to exhibit reentrant behavior as the chemical potential changes [20]. Perturbative studies of two Kondo impurities in graphene indicate that generic competition between Kondo screening and the RKKY interaction persists even with

Landau levels being present [20–25]. Nonetheless, the complete phase diagram and behaviors of relevant physical quantities such as entropy, specific heat, and susceptibility are still unknown.

Theoretically, in the absence of Landau levels, the numerical renormalization group (NRG) method has provided a more complete description of the Kondo screening than the mean-field and perturbation approaches [24]. In this paper, we borrow the iterative diagonalization procedure from the NRG method to investigate one and two magnetic impurities screened by discrete Landau levels at zero temperature. We will show that the ground state generally oscillates in Kondo screening state and partially screened and unscreened spin states. This leads to quantum oscillations observed in magnetization of the system. In particular, we find that two impurities in the ground state can form spin-0 (singlet) and spin-1 (triplet) states. Remarkably, these states can be either screened, partially screened, or unscreened with the emergence of these states being oscillating with the change of magnetic field, chemical potential, or interimpurity distance. Our results indicate that the oscillation in Kondo screening phases is the key to understanding the observed quantum oscillation in Kondo systems.

II. MODEL HAMILTONIANS

We start by considering the two-dimensional multi-impurities Anderson model with the magnetic field $\vec{B}$ being along the z direction. By treating the conduction electron in the continuum limit, the Hamiltonian can be written as

$$\begin{aligned} H &= H_c + H_d + H_V, \\ H_c &= \int d\vec{r} \sum_\sigma c^\dagger_{\vec{r}\sigma}\left(\frac{\vec{\Pi}^2}{2m_e^*} - \mu\right)c_{\vec{r}\sigma} + g_c\mu_B B s^z_{c,\vec{r}}, \\ H_d &= U\sum_j n^d_{j\uparrow}n^d_{j\downarrow} + \sum_{j\sigma}\xi^d n^d_{j\sigma} + g_d\mu_B B\sum_j s^z_{d,j}, \\ H_V &= Va\int d\vec{r}\sum_{j\sigma}\delta\left(\vec{r}-\vec{r}^{\,d}_j\right)\left(d^\dagger_{j\sigma}c_{\vec{r}\sigma} + \text{H.c.}\right). \end{aligned} \tag{1}$$

Here H_c is the Hamiltonian for describing the conduction electrons, H_d is the Hamiltonian for describing the impurities' electrons, and H_V is describing the hybridization between conduction and impurity's electrons. $\vec{\Pi} = \vec{p} + e\vec{A}/c$ is the kinetic momentum operator with $\vec{A}$ being the vector potential for $\vec{B}$, μ is the chemical potential, m_e^* is the effective mass of the electron, a^2 is the effective area of impurity hybridization range, g_c and g_d are the g factors of conduction and impurities' electrons, and V is the hybridization strength between impurities and conduction electrons. $c^\dagger_{\vec{r}\sigma}$ and $d^\dagger_{j\sigma}$ are the creation operators for conduction electrons at position $\vec{r} = (x^d_j, y^d_j)$ and localized electrons at position $\vec{r}^{\,d}_j$ with spin σ, respectively. $s^z_{c,\vec{r}} = \frac{1}{2}(c^\dagger_{\vec{r}\uparrow}c_{\vec{r}\uparrow} - c^\dagger_{\vec{r}\downarrow}c_{\vec{r}\downarrow})$ and $s^z_{d,j} = \frac{1}{2}(d^\dagger_{j\uparrow}d_{j\uparrow} - d^\dagger_{j\downarrow}d_{j\downarrow})$ are spin operators for conduction and impurities' electrons, respectively. In the Landau gauge $\vec{A} = (0, Bx, 0)$, the single-particle eigenenergy and the corresponding eigenfunction of the conduction electrons are

$$\begin{aligned} \varepsilon^c_n &= \varepsilon_B\left(n+\frac{1}{2}\right), \quad \xi^c_n = \varepsilon^c_n - \mu, \\ \psi_{n,k_y}(\vec{r}) &= \frac{e^{-ik_y y}}{\sqrt{L}}\phi_n(x+x_k), \quad x_k = l_B^2 k_y, \\ \phi_n(x) &= \frac{1}{\sqrt{2^n n!\pi^{1/2}l_B}}H_n(x/l_B)e^{-x^2/(2l_B^2)}, \end{aligned} \tag{2}$$

where $\varepsilon_B = \hbar\omega_B$ is the Landau quantized energy with $\omega_B = eB/(m_e^* c)$ being the cyclotron frequency, k_y is the wave vector along the y direction, $l_B = \sqrt{\hbar/(m_e^*\omega_B)} = \sqrt{c\hbar/(eB)}$ is the magnetic length, and $H_n(x)$ is the nth Hermite polynomial. The magnetic length l_B is approximated to $25.7\ \text{nm}/\sqrt{B(\text{T})}$, where $B(\text{T})$ represents the magnetic field (B is unit of Tesla). The restriction of $-L/2 \leqslant x_k \leqslant L/2$ gives the allowed states number of k_y as Landau degeneracy

$$N_L = L^2/\left(2\pi l_B^2\right) = L^2\frac{m_e^*}{2\pi\hbar^2}\varepsilon_B = L^2\rho\varepsilon_B, \tag{3}$$

where L is the length of square system, and $\rho = m_e^*/(2\pi\hbar^2)$ is the density of states of two-dimensional free-electron gas with effective mass m_e^*.

By using $\psi_{n,k_y}(\vec{r})$, we can transform the annihilation operator to the basis of the Landau quantized states as

$$\begin{aligned} c_{nk_y\sigma} &= \int d\vec{r}\ \psi_{n,k_y}(\vec{r})c_{\vec{r}\sigma}, \\ c_{\vec{r}\sigma} &= \sum_{nk_y}\psi^*_{n,k_y}(\vec{r})c_{nk_y\sigma}. \end{aligned} \tag{4}$$

After applying the transformation, the Hamiltonian projected in Landau eigenstates is given by

$$\begin{aligned} H = H_d &+ \sum_{\{n\},k_y\sigma}\xi^c_{n\sigma}c^\dagger_{nk_y\sigma}c_{nk_y\sigma} \\ &+ \frac{\tilde{V}}{\sqrt{L}}\sum_{j\{n\},k_y\sigma}e^{ik_y y^d_j}\phi_n\left(x^d_j + x_k\right)d^\dagger_{j\sigma}c_{nk_y\sigma} + \text{H.c.} \end{aligned} \tag{5}$$

Here $\tilde{V} = Va$, $\xi^c_{n\uparrow} = \xi^c_n + g_c\mu_B B/2$, $\xi^c_{n\downarrow} = \xi^c_n - g_c\mu_B B/2$, and we also take an energy cutoff D so that $\xi^c_n = \varepsilon^c_n - \mu \in [-D, D]$ and $n = \{N_{\min}, N_{\min}+1, \ldots, N_{\max}\}$ with $N_{\max}$ being the maximum number and $N_{\min}$ being the minimum number of the Landau level index n.

A. Reduction in degrees of freedom for conduction electrons coupling with impurities

Before further simplifying the Hamiltonian, we shall first show that degrees of freedom for conduction electrons coupling with impurities can be reduced. This is illustrated by considering a toy model in which an impurity couples to two degenerate one-dimensional chains X_n and Y_n, with the Hamiltonian

$$\begin{aligned} H_T = H_d &+ \sum_{\{n\},\sigma}\xi_{n\sigma}\left(X^\dagger_{n\sigma}X_{n\sigma} + Y^\dagger_{n\sigma}Y_{n\sigma}\right) \\ &+ \sum_{\{n\},\sigma}d^\dagger_\sigma\left(V_X X_{n\sigma} + V_Y Y_{n\sigma}\right) + \text{H.c.} \end{aligned} \tag{6}$$

By defining two new operators

$$A_{n\sigma} = \frac{1}{\sqrt{V_X^2+V_Y^2}}(V_X X_{n\sigma} + V_Y Y_{n\sigma}),$$
$$B_{n\sigma} = \frac{1}{\sqrt{V_X^2+V_Y^2}}(-V_Y X_{n\sigma} + V_X Y_{n\sigma}), \quad (7)$$

it is then easy to see that $A_{n\sigma}$ and $B_{n\sigma}$ obey fermionic commutation relations: $\{A_{n\sigma}^\dagger, A_{n\sigma}\} = \{B_{n\sigma}^\dagger, B_{n\sigma}\} = 1$, $\{A_{n\sigma}^\dagger, B_{n\sigma}\} = \{A_{n\sigma}, B_{n\sigma}\} = 0$. The Hamiltonian H_T can be rewritten as

$$H_T = H_d + \sum_{\{n\},\sigma} \xi_{n\sigma}(A_{n\sigma}^\dagger A_{n\sigma} + B_{n\sigma}^\dagger B_{n\sigma}) + \sqrt{V_X^2+V_Y^2}\sum_{\{n\},\sigma} d_\sigma^\dagger A_{n\sigma} + \text{H.c.} \quad (8)$$

Clearly, we see that the operator $B_{n\sigma}$ decouples from the impurity and only $A_{n\sigma}$ couples to the impurity with a stronger hybridization strength $\sqrt{V_X^2+V_Y^2}$. Effectively, degrees of freedom for conduction electrons coupling with impurities are reduced.

Going back to the Hamiltonian (5), the impurity operator $d_{j\sigma}^\dagger$ also couples to two degenerated state operators X_n and Y_n with a two-dimensional hybridization vector $\vec{V} = (V_X, V_Y)$. Hence, similar reduction of degrees of freedom can be performed (see the following subsection). In general, if the conduction electrons possess more degeneracies characterized by N_L [$N_L = 2$ for H_T, for Landau levels, N_L is the Landau degeneracy given by Eq. (3)], the coupling of conduction electrons to a single impurity can be characterized by a N_L-dimensional hybridization vector $\vec{V}$. By performing similar analysis, it is clear that an impurity effectively only couples to one channel with hybridization strength $\|\vec{V}\|$. Furthermore, if there are N_{imp} impurities operators $d_j^\dagger$ coupling to N_L degenerated conduction electrons with the hybridization vector $\vec{V}_j$, these impurities effectively couple to $N_L - N_{\text{imp}}$ channel when $N_L \geqslant N_{\text{imp}}$.

B. Reduced single-impurity Hamiltonian H_1

We start with the single-impurity case with the position of the impurity being at $(0, R)$. The hybridization between the impurity and conduction electrons is given by

$$H_V = \frac{\tilde{V}}{\sqrt{L}}\sum_{\{n\},k_y\sigma} \phi_n(x_k) e^{ik_y R} d_\sigma^\dagger c_{nk_y\sigma} + \text{H.c.} \quad (9)$$

By collecting annihilation operators which couple to the impurity and redefining them as a new operator as

$$x_n A_{n\sigma} = \sqrt{\frac{L}{N_L}}\sum_{k_y} e^{ik_y R}\phi_n(x_k) c_{nk_y\sigma}, \quad (10)$$

where $x_n = \sqrt{\frac{L}{N_L}\sum_{k_y}|e^{ik_y R}\phi_n(x_k)|^2}$ is the normalization constant. The new hybridization term becomes $\tilde{V}\sqrt{\rho\varepsilon_B}\sum_{\{n\}\sigma}(x_n d_\sigma^\dagger A_{n\sigma} + \text{H.c.})$. According to the analysis in Sec. II A, it is clear that the impurity only hybridizes to $A_{n\sigma}$ and decouples from the remaining $N_L - 1$ states if $N_L \geqslant 1$.

To obtain the normalized constant x_n, we first note that the dimensionless function

$$\bar{\phi}_n(x/l_B) = \sqrt{l_B}\phi_n(x) = \frac{1}{\sqrt{2^n n!\pi^{1/2}}} H_n(x/l_B) e^{-x^2/(2l_B^2)} \quad (11)$$

satisfies the normalization condition $\int_{-\infty}^{\infty} dt\, \bar{\phi}_n^2(t) = 1$. For $L \gg l_B$, the normalized constant x_n can be simplified as follows:

$$x_n = \sqrt{\frac{L}{N_L}\sum_{k_y}\phi_n^2(x_k)} = \sqrt{\frac{L^2}{2\pi N_L}\int_{k_y^{\min}}^{k_y^{\max}} dk_y \phi_n^2(x_k)}$$
$$= \sqrt{\int_{-\frac{L}{2}}^{\frac{L}{2}} dx_k \phi_n^2(x_k)} = \sqrt{\int_{-\infty}^{\infty} dt\, \bar{\phi}_n^2(t)} = 1, \quad (12)$$

where $t = x/l_B$. Thus, we obtain the hybridization term in the new basis as $(\rho\tilde{V}^2\varepsilon_B)^{1/2}\sum_{\{n\}\sigma}(d_\sigma^\dagger A_{n\sigma} + \text{H.c.})$. As a result, the reduced single-impurity Hamiltonian H_1 in terms of $A_{n,\sigma}^\dagger$ is given by

$$H_1 = U d_\uparrow^\dagger d_\uparrow d_\downarrow^\dagger d_\downarrow + \sum_\sigma \xi_\sigma^d d_\sigma^\dagger d_\sigma + \sum_{\{n\},\sigma}\xi_{n\sigma}^c A_{n\sigma}^\dagger A_{n\sigma} + \left(\frac{\Gamma\varepsilon_B}{\pi}\right)^{1/2}\left(\sum_{\{n\},\sigma} d_\sigma^\dagger A_{n\sigma} + \text{H.c.}\right), \quad (13)$$

where $\Gamma = \pi\rho V^2$. It is important to note that only one channel in the Landau level couples to the impurity in H_1.

C. Reduced two-impurities Hamiltonian H_2

In the two-impurities case, positions of impurities are set at $(0, \pm R/2)$. For general positions, please see the Supplemental Material [26]. The hybridization between impurities and conduction electrons is given by

$$\frac{\tilde{V}}{\sqrt{L}}\sum_{\{n\},k_y\sigma}\phi_n(x_k)\left(e^{ik_y R/2} d_{1\sigma}^\dagger + e^{-ik_y R/2} d_{2\sigma}^\dagger\right) c_{nk_y\sigma} + \text{H.c.} \quad (14)$$

Hence, for impurity 1, the impurity operator $d_{1\sigma}^\dagger$ couples to $\sqrt{L/N_L}\sum_{k_y} e^{ik_y R/2}\phi_n(x_k)c_{nk_y\sigma}$, while for impurity 2, the impurity operator $d_{2\sigma}^\dagger$ couples to $\sqrt{L/N_L}\sum_{k_y} e^{-ik_y R/2}\phi_n(x_k)c_{nk_y\sigma}$. It is easy to see that the overlap of the coefficients in the above operators is nonvanishing

$$\int_{-\infty}^{\infty} dt \left(e^{-it(R/2l_B)}\bar{\phi}_n(t)\right)^* e^{it(R/2l_B)}\bar{\phi}_n(t) = \int_{-\infty}^{\infty} dt\, e^{i\eta t}\bar{\phi}_n^2(t) \neq 0, \quad (15)$$

where $\eta = R/l_B$. Hence, these operators are not orthogonal when $L \gg l_B$. However, if we define

$$x_n A_{n\sigma} = \sqrt{\frac{L}{N_L}}\sum_{k_y}\cos(k_y R/2)\phi_n(x_k)c_{nk_y\sigma},$$
$$y_n B_{n\sigma} = \sqrt{\frac{L}{N_L}}\sum_{k_y} i\,\sin(k_y R/2)\phi_n(x_k)c_{nk_y\sigma}, \quad (16)$$

where x_n and y_n are normalization constants to be determined, we shall see that by fixing x_n and y_n correctly, $A_{n\sigma}$ and $B_{n\sigma}$ are two orthogonal annihilation operators with standard fermion commutation relations. First, note that because the following integral vanishes

$$\int_{-\infty}^{\infty} dt\ \sin\left(\frac{\eta t}{2}\right)\cos\left(\frac{\eta t}{2}\right)\bar{\phi}_n^2(t) = \frac{1}{2}\int_{-\infty}^{\infty} dt\ \sin(\eta t)\bar{\phi}_n^2(t) = 0, \tag{17}$$

we have $\{A_{n\sigma}^\dagger, B_{n\sigma}\} = 0$ when $L \gg l_B$. The normalization constants x_n and y_n are determined by the required commutation relations and are given by [26]

$$\begin{aligned} x_n &= \sqrt{\frac{1}{2}\int_{-\infty}^{\infty} dt\ \cos^2\frac{\eta t}{2}\bar{\phi}_n^2(t)} = \sqrt{\frac{1+u_n}{2}}, \\ y_n &= \sqrt{\frac{1}{2}\int_{-\infty}^{\infty} dt\ \sin^2\frac{\eta t}{2}\bar{\phi}_n^2(t)} = \sqrt{\frac{1-u_n}{2}}, \\ u_n &= \mathrm{Re}\left(\int_{-\infty}^{\infty} dt\, e^{i\eta t}\bar{\phi}_n^2(t)\right) = e^{-\eta^2/4}L_n(\eta^2/2), \end{aligned} \tag{18}$$

where $L_n(x)$ is the nth Laguerre polynomial. Thus, the effective hybridization becomes

$$\begin{aligned} &(\rho\tilde{V}^2\varepsilon_B)^{1/2}[d_{1\sigma}^\dagger(x_nA_{n\sigma} + y_nB_{n\sigma}) \\ &\quad + d_{2\sigma}^\dagger(x_nA_{n\sigma} - y_nB_{n\sigma}) + \text{H.c.}]. \end{aligned} \tag{19}$$

The reduced two-impurities Hamiltonian H_2 in terms of $A_{n,\sigma}^\dagger$ and $B_{n,\sigma}^\dagger$ is then given by

$$\begin{aligned} H_2 = {} & U\sum_{j=1,2} d_{j\uparrow}^\dagger d_{j\uparrow} d_{j\downarrow}^\dagger d_{j\downarrow} + \sum_{j=1,2,\sigma}\xi_\sigma^d d_{j\sigma}^\dagger d_{j\sigma} \\ & + \sum_{\{n\},\sigma}\xi_{n\sigma}^c(A_{n\sigma}^\dagger A_{n\sigma} + B_{n\sigma}^\dagger B_{n\sigma}) \\ & + \left(\frac{\Gamma\varepsilon_B}{\pi}\right)^{1/2}\sum_{\{n\},\sigma}[(d_{1\sigma}^\dagger + d_{2\sigma}^\dagger)x_nA_{n\sigma} \\ & + (d_{1\sigma}^\dagger - d_{2\sigma}^\dagger)y_nB_{n\sigma} + \text{H.c.}]. \end{aligned} \tag{20}$$

Note that if we redefine new operators $X_{n\sigma}$ and $Y_{n\sigma}$ by performing an orthogonal transformation between $A_{n\sigma}$ and $B_{n\sigma}$ as

$$X_n = x_nA_{n\sigma} + y_nB_{n\sigma},\ Y_n = -y_nA_{n\sigma} + x_nB_{n\sigma}, \tag{21}$$

the hybridization shown in Eq. (19) becomes

$$(\rho\tilde{V}^2\varepsilon_B)^{1/2}\left(d_{1\sigma}^\dagger X_{n\sigma} + d_{2\sigma}^\dagger\left(u_nX_{n\sigma} - \sqrt{1-u_n^2}Y_{n\sigma}\right) + \text{H.c.}\right). \tag{22}$$

It is clear from the above form of hybridization that when all u_n vanish, two impurities decouple and the system is the same as the case for a single impurity, while if all u_n are equal to 1, both the impurity operators couple to the same operator $X_{n\sigma}$, the system thus becomes the well-known two-impurity–one-channel Kondo problem. In Fig. 1, we show how u_n depends on the dimensionless interimpurity distance η. Clearly, neither all u_n vanish nor u_n are all equal to 1. Hence, two impurities in the Anderson model are a two-channel problem.

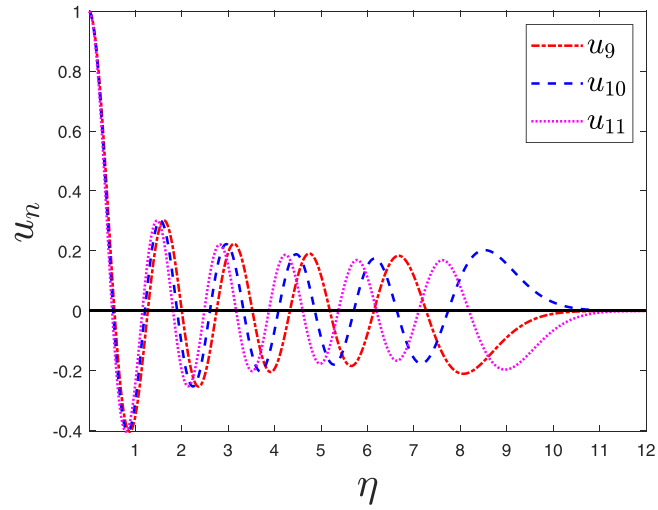

FIG. 1. Illustration of u_n versus $\eta = R/l_B$ for $n = 9$, 10, and 11, where R is the distance between two impurities and l_B is the magnetic length.

III. ITERATIVE DIAGONALIZATION

In this section, we will describe how to use the numerical iterative diagonalization procedure adopted in the method of NRG to analyze the Kondo effect in strong magnetic fields. We emphasize that our calculation focuses on the low-energy states at final iteration, which correspond to the low-energy states of reduced Hamiltonian H_1 or H_2. At each iteration, the iterative procedure disregards high-energy states. The convergence of our results indicates the energy scale separation of high- and low-energy modes.

A. Transform diagonal matrix into hopping matrix

The first step of the iterative diagonalization is to transform the diagonalized Hamiltonian of conduction electron into hopping Hamiltonian. Explicitly, it means to find the hopping energy t_m, atomic energy ϵ_m, and the transformation $A_{n\sigma} = u_{n,m}f_{m\sigma}$, such that the kinetic energy $\sum_{n\sigma}\xi_{n\sigma}^c A_{n\sigma}^\dagger A_{n\sigma}$ in Eq. (20) becomes

$$\begin{aligned} &\sum_{n\sigma}\xi_{n\sigma}^c A_{n\sigma}^\dagger A_{n\sigma} \\ &\quad = \sum_{m=1,\sigma}^{N_t}\epsilon_m f_{m\sigma}^\dagger f_{m\sigma} + t_m(f_{m\sigma}^\dagger f_{m+1\sigma} + \text{H.c.}). \end{aligned} \tag{23}$$

Here we have renumbered the Landau-level index n from the original range $(N_{\min}, N_{\max})$ to $(1, N_t)$ with the understanding that the energy of the Landau level changes to $\varepsilon_n^c = \varepsilon_B(n - 1 + N_{\min} + \frac{1}{2})$. $\{u_{n,m}\}$ is the transformation matrix transforming $A_{n\sigma}$ to $f_{n\sigma}$. As the impurity operators $d_{1\sigma}^\dagger$ and $d_{2\sigma}^\dagger$ are already put at site 1 [see Eq. (22)], $u_{n,1}$ is given by the coupling coefficient to the impurity. For the remaining components $u_{n,m}$, we consider a vector $v_{m,n}$ for fixed n as the eigenvector to the Hamiltonian with hopping t_m and onsite energy ϵ_m such

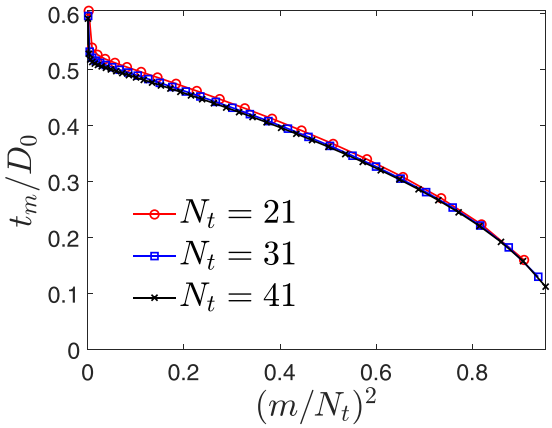

FIG. 2. The hopping amplitudes t_m follow the scaling form $t_m/D = f(m/N_t)$ with $f(x)$ being roughly in the form of $a - bx$.

that $v_{m,n}$ satisfies

$$\begin{pmatrix} \epsilon_1 & t_1 & \\ t_1 & \epsilon_2 & t_2 \\ & t_2 & \dots \end{pmatrix} \begin{pmatrix} v_{1,n} \\ v_{2,n} \\ \dots \end{pmatrix} = \xi_n \begin{pmatrix} v_{1,n} \\ v_{2,n} \\ \dots \end{pmatrix}. \tag{24}$$

Here, ξ_n is the eigenvalue. Clearly, the desired transformation $\{u_{n,m}\}$ is given by $u_{n,m} = v_{m,n}$. Hence, $v_{1,n} = u_{n,1}$. From Eq. (24), it is easy to find the recurrence relation for $v_{m,n}$:

$$\begin{aligned} t_m v_{m+1,n} &= (\xi_n - \epsilon_m) v_{m,n} - t_{m-1} v_{m-1,n}, \\ &\quad \text{for } 1 < m < N_t \\ t_1 v_{2,n} &= (\xi_n - \epsilon_1) v_{1,n}, \\ t_{N_t} v_{N_t-1,n} &= (\xi_n - \epsilon_{N_t}) v_{N_t,n}. \end{aligned} \tag{25}$$

$v_{m,n}$ (and thus $u_{n,m}$) can be found by the initial condition $v_{1,n} = u_{n,1}$. The orthogonality requirement of transformation $\hat{v} = (v_{mn})$ is $\hat{v}\hat{v}^T = I$, i.e., $\sum_n v_{m,n} v_{m',n} = \delta_{m,m'}$. Hence, by multiplying $v_{m,n}$ in Eq. (25) and summing over n, we find

$$\epsilon_m = \sum_n \xi_n^2 v_{m,n}^2. \tag{26}$$

By using Eqs. (25) and (26), $v_{1,n}$, and the normalized condition $\sum_n v_{m,n}^2 = 1$, all $v_{m,n}$ and t_m can be determined numerically. Numerically, as shown in Fig. 2, we find that for a single impurity, $\epsilon_m = 0$ and t_m follows a scaling form $t_m/D = f(m/N_t)$ with $f(x)$ being roughly in the form of $a - bx$. Furthermore, we find that for $N_t \gtrsim 36$, due to the accumulation of numerical error that includes the error introduced by diagonalization in each recurrence step, the orthogonality of the first and final states is poor. Hence, in our calculation, we limit our calculations to systems with $N_t < 30$ so that the absolute value of the inner product between first and final states $< 10^{-10}$. The error generated from this step can be neglected, as it is the order 10^{-10} of ε_B when comparing the eigenvalue of hopping matrix with the original diagonal matrix. Note that t_m does not decay exponentially but exhibits a square-root-like decay form for large m as indicated in the Supplemental Material [26]. The accuracy problem related to the decay form of t_m will be discussed in the last subsection of this section.

B. Effective 1D chain Hamiltonians for single impurity and two impurities

The transformation of single-impurity Hamiltonian H_1 into an effective one-dimensional (1D) chain Hamiltonian can be achieved by setting the new annihilation operator $f_{1\sigma} = \frac{1}{\sqrt{N_t}} \sum_n A_{n\sigma}$ with $N_t = N_{\max} - N_{\min} + 1$ being the total number of Landau levels within the energy cutoff. This gives $u_{n,1} = \frac{1}{\sqrt{N_t}}$. With $\xi_n = \varepsilon_B(n - 1 + N_{\min} + \frac{1}{2}) - \mu$ and $u_{n,1}$, t_m and ε_m can be obtained by solving Eqs. (25) and (26). After the transformation, we obtained the single-impurity 1D chain Hamiltonian as

$$\begin{aligned} H_1^W &= U d_\uparrow^\dagger d_\uparrow d_\downarrow^\dagger d_\downarrow + \sum_\sigma \xi_\sigma^d d_\sigma^\dagger d_\sigma + \bar{\Gamma} \sum_\sigma (d_\sigma^\dagger f_{1\sigma} + \text{H.c.}) \\ &\quad + \sum_{m=1,\sigma}^{N_t} \epsilon_{m\sigma} f_{m\sigma}^\dagger f_{m\sigma} + \sum_{m=1,\sigma}^{N_t-1} t_m (f_{m\sigma}^\dagger f_{m+1\sigma} + \text{H.c.}), \end{aligned} \tag{27}$$

where the effective coupling between the impurity electrons and conduction electrons is $\bar{\Gamma} = (\frac{\Gamma \varepsilon_B}{\pi})^{1/2} N_t^{1/2}$. Similarly, the transformation of the two-impurities Hamiltonian H_2 can be achieved by setting $f_{1\sigma} = \frac{1}{\sqrt{\sum_n x_n^2}} \sum_n x_n A_{n\sigma}$ and $g_{1\sigma} = \frac{1}{\sqrt{\sum_n y_n^2}} \sum_n y_n B_{n\sigma}$. The resulting two-impurities 1D chain Hamiltonian is given by

$$\begin{aligned} H_2^W &= U \sum_{j=1,2} d_{j\uparrow}^\dagger d_{j\uparrow} d_{j\downarrow}^\dagger d_{j\downarrow} + \sum_{j=1,2,\sigma} \xi_\sigma^d d_{j\sigma}^\dagger d_{j\sigma} \\ &\quad + \sum_{m=1,\sigma}^{N_t} \epsilon_{m\sigma}^f f_{m\sigma}^\dagger f_{m\sigma} + \epsilon_{m\sigma}^g g_{m\sigma}^\dagger g_{m\sigma} \\ &\quad + \sum_{m=1,\sigma}^{N_t-1} \left(t_m^f f_{m\sigma}^\dagger f_{m+1\sigma} + t_m^g g_{m\sigma}^\dagger g_{m+1\sigma} + \text{H.c.} \right) \\ &\quad + \sum_\sigma \bar{\Gamma}_f (d_{1\sigma}^\dagger + d_{2\sigma}^\dagger) f_{1\sigma} + \bar{\Gamma}_g (d_{1\sigma}^\dagger - d_{2\sigma}^\dagger) g_{1\sigma} + \text{H.c.}, \end{aligned} \tag{28}$$

where the effective couplings are $\bar{\Gamma}_f = (\Gamma \varepsilon_B / \pi \sum_{\{n\}} x_n^2)^{1/2}$ and $\bar{\Gamma}_g = (\Gamma \varepsilon_B / \pi \sum_{\{n\}} y_n^2)^{1/2}$.

Finally, the procedure for transformation of the reduced Hamiltonian H_1 and H_2 to an effective 1D chain Hamiltonian H_w is schematically illustrated in Fig. 3.

C. Details of the 1D chain model calculation

Details of iteratively diagonalizing a single-impurity one-channel Hamiltonian H_1^W is well known [24,27]. We will only show details of iteratively diagonalizing a two- or higher-channel Hamiltonian. We start with H_2^W shown in Eq. (28), and relabel $d_{1\sigma} = P_{-1\sigma}$, $d_{2\sigma} = P_{0\sigma}$, $f_{m\sigma} = P_{2m-1\sigma}$, $g_{m\sigma} = P_{2m\sigma}$. Then the Hamiltonian includes the Hubbard terms $P_{-1\uparrow}^\dagger P_{-1\uparrow} P_{-1\downarrow}^\dagger P_{-1\downarrow}$, $P_{0\uparrow}^\dagger P_{0\uparrow} P_{0\downarrow}^\dagger P_{0\downarrow}$, the charge terms $\sum_\sigma P_{n\sigma}^\dagger P_{n\sigma}$, the Zeeman interaction terms $P_{0\uparrow}^\dagger P_{0\uparrow} - P_{0\downarrow}^\dagger P_{0\downarrow}$, and several hopping terms such as $P_{n\sigma}^\dagger P_{n+1\sigma} + \text{H.c.}$, $P_{n\sigma}^\dagger P_{n+2\sigma} + \text{H.c.}$, and $P_{n\sigma}^\dagger P_{n+3\sigma} + \text{H.c.}$ The Hamiltonian is the summation of these terms and commutes with total charge $\hat{Q}_N$

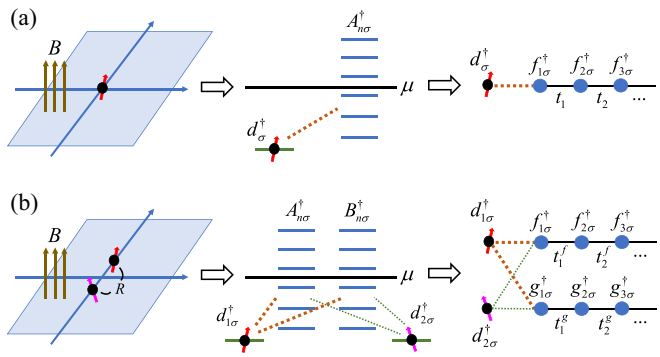

FIG. 3. A schematic diagram shows steps for transforming the multi-impurity Anderson model to the effective 1D chain Hamiltonian for (a) a single impurity and (b) two impurities.

and the z component of total spin $\hat{S}^z_N$, which are given by

$$\hat{Q}_N = \sum_n^N (P^\dagger_{n\uparrow}P_{n\uparrow} + P^\dagger_{n\downarrow}P_{n\downarrow} - 1),$$
$$\hat{S}^z_N = \sum_{n,\sigma\sigma'}^N P^\dagger_{n\sigma}\frac{\tau^z_{\sigma\sigma'}}{2}P_{n\sigma'}. \tag{29}$$

Here τ^z is the z component of the Pauli matrices. N is number of $P^\dagger_\sigma$ operators of any chain Hamiltonian. Hence, the Hamiltonian is block diagonalized by using the basis specified by quantum numbers Q and S_z. Furthermore, each block in the Hamiltonian is specified by the quantum number (Q, S_z) with the energy eigenstates for each block being represented by $|Q, S_z, r\rangle_N$, where $r = 1, 2, 3, \ldots$ is the ordering of the eigenstates in each block. In addition, when two impurities have the same strength in Hubbard interaction and atomic energy, H^W_2 possess additional parity symmetry. In order to apply this symmetry in diagonalization, it is more convenient to rearrange operators in H^W_2 by using even or odd representations of operators defined by

$$d_{e\sigma} = \frac{1}{\sqrt{2}}(d_{1\sigma} + d_{2\sigma}), \quad d_{o\sigma} = \frac{1}{\sqrt{2}}(d_{1\sigma} - d_{2\sigma}),$$
$$c_{m,e\sigma} = f_{m\sigma}, \quad c_{m,o\sigma} = g_{m\sigma}, \tag{30}$$

where the subscript e labels even and o labels odd parity. H^W_2 then becomes

$$\begin{aligned} H^W_2 = {} & \frac{U}{2}[(d^\dagger_{e\uparrow}d_{e\uparrow} + d^\dagger_{o\uparrow}d_{o\uparrow})(d^\dagger_{e\downarrow}d_{e\downarrow} + d^\dagger_{o\downarrow}d_{o\downarrow})] \\ & + \frac{U}{2}[(d^\dagger_{e\uparrow}d_{o\uparrow} + d^\dagger_{o\uparrow}d_{e\uparrow})(d^\dagger_{e\downarrow}d_{o\downarrow} + d^\dagger_{o\downarrow}d_{e\downarrow})] \\ & + \sum_\sigma \xi^d_\sigma (d^\dagger_{e\sigma}d_{e\sigma} + d^\dagger_{o\sigma}d_{o\sigma}) \\ & + \sum_{m=1,\sigma}^{N_t} \epsilon^f_{m\sigma} c^\dagger_{m,e\sigma}c_{m,e\sigma} + \epsilon^g_{m\sigma} c^\dagger_{m,o\sigma}c_{m,o\sigma} \\ & + \sum_{m=1,\sigma}^{N_t-1} \left(t^f_m c^\dagger_{m,e\sigma}c_{m+1,e\sigma} + t^g_m c^\dagger_{m,o\sigma}c_{m+1,o\sigma} + \text{H.c.}\right) \\ & + \sum_\sigma \sqrt{2}\bar{\Gamma}_f d^\dagger_{e\sigma}c_{1,e\sigma} + \sqrt{2}\bar{\Gamma}_g d^\dagger_{o\sigma}c_{1,o\sigma} + \text{H.c.} \end{aligned} \tag{31}$$

Using the relabeling notations $d_{e\sigma} = P_{-1\sigma}$, $d_{o\sigma} = P_{0\sigma}$, $c_{m,e\sigma} = P_{2m-1\sigma}$, $c_{m,o\sigma} = P_{2m\sigma}$, the parity operator is given by $\hat{P}_N = (-1)^{\hat{O}_N}$, where

$$\hat{O}_N = \sum_{n=\text{even},\sigma} P^\dagger_{n\sigma}P_{n\sigma}. \tag{32}$$

Note that for a single impurity, one uses the quantum number (Q, S_z) to perform iterative diagonalization, while for two impurities, one can either use (Q, S_z) or (Q, S_z, P) for iterative diagonalization. In the following, we will present the formalism of the Hamiltonian involved in each iteration by using either the set of quantum number (Q, S_z) or (Q, S_z, P).

1. Iterative diagonalization in (Q, S_z) basis

Let $|Q, S_z, r\rangle_N$ denote eigenstates of H_N such that

$$H_N|Q, S_z, r\rangle_N = E_N(Q, S_z, r)|Q, S_z, r\rangle_N, \tag{33}$$

where $r = 1, 2, 3, \ldots$ labels the ordering of the eigenstates in each block specified by Q and S_z.

When adding a new site with fermion operator $P^\dagger_{N+1\sigma}$, new states have to include extra particles (holon, one particle, or two particles) at the new site so that we define new basis states as follows:

$$\begin{aligned} |q, r, 1\rangle_{N+1} &\equiv |0; Q+1, S_z, r\rangle_N, \\ |q, r, 2\rangle_{N+1} &\equiv \left|\uparrow_{N+1}; Q, S_z - \tfrac{1}{2}, r\right\rangle_N, \\ |q, r, 3\rangle_{N+1} &\equiv \left|\downarrow_{N+1}; Q, S_z + \tfrac{1}{2}, r\right\rangle_N, \\ |q, r, 4\rangle_{N+1} &\equiv |\uparrow\downarrow_{N+1}; Q-1, S_z, r\rangle_N, \end{aligned} \tag{34}$$

where we collectively denote the quantum number $(Q+1, S_z)$ by q and the relevant states on the right-hand side are defined by using $P^\dagger_{N+1\sigma}$ as

$$\begin{aligned} |0; Q+1, S_z, r\rangle_N &\equiv |Q+1, S_z, r\rangle_N, \\ \left|\uparrow_{N+1}; Q, S_z - \tfrac{1}{2}, r\right\rangle_N &\equiv P^\dagger_{N+1\uparrow}\left|Q, S_z - \tfrac{1}{2}, r\right\rangle_N, \\ \left|\downarrow_{N+1}; Q, S_z + \tfrac{1}{2}, r\right\rangle_N &\equiv P^\dagger_{N+1\downarrow}\left|Q, S_z + \tfrac{1}{2}, r\right\rangle_N, \\ |\uparrow\downarrow_{N+1}; Q-1, S_z, r\rangle_N &\equiv P^\dagger_{N+1\uparrow}P^\dagger_{N+1\downarrow}|Q-1, S_z, r\rangle_N. \end{aligned}$$

Note that $|q, r, i\rangle_N$ can be also written in the form $|Q, S_z, r, i\rangle_N$, and the states $|q, r, i\rangle_N$ with $i = 1, 2, 3$, and 4 are built from energy eigenstates $|Q, S_z, r\rangle_{N-1}$ with the number of sites being $N-1$ but they are not energy eigenstates for the number of sites being N.

The Hamiltonian with an extra site is given by $H_{N+1} = H_N + H^I_{N,1}$, where the nonvanishing matrix elements of hopping Hamiltonian in the same block labeled by (Q, S_z), $H^I_{N,1} = \sum_\sigma P^\dagger_{N\sigma}P_{N+1\sigma} + \text{H.c.}$, can be expressed as matrix elements of $P^\dagger_{N\sigma}$ in the basis of energy eigenstates:

$$\begin{aligned} \langle q, r, 1|H^I_{N,1}|q, r', 2\rangle_{N+1} &= \langle Q+1, S_z, r|P^\dagger_{N\uparrow}\left|Q, S_z - \tfrac{1}{2}, r'\right\rangle_N, \\ \langle q, r, 3|H^I_{N,1}|q, r', 4\rangle_{N+1} &= -\left\langle Q, S_z + \tfrac{1}{2}, r\right|P^\dagger_{N\uparrow}|Q-1, S_z, r'\rangle_N, \\ \langle q, r, 1|H^I_{N,1}|q, r', 3\rangle_{N+1} &= \langle Q+1, S_z, r|P^\dagger_{N\downarrow}\left|Q, S_z + \tfrac{1}{2}, r'\right\rangle_N, \\ \langle q, r, 2|H^I_{N,1}|q, r'4\rangle_{N+1} &= \left\langle Q, S_z - \tfrac{1}{2}, r\right|P^\dagger_{N\downarrow}|Q-1, S_z, r'\rangle_N. \end{aligned} \tag{35}$$

Hence, we need to calculate $\langle Q, S_z, r|P^\dagger_{N\sigma}|Q', S'_z, r'\rangle_N$. For this purpose, we first note the following identities by using the definition of $|Q, S_z, r, i\rangle_N$:

$$\begin{aligned}
&\left\langle Q+1, S_z+\tfrac{1}{2}, r, 2\right|P^\dagger_{N\uparrow}|Q, S_z, r, 1\rangle_N = 1,\\
&\left\langle Q+1, S_z+\tfrac{1}{2}, r, 4\right|P^\dagger_{N\uparrow}|Q, S_z, r, 3\rangle_N = 1,\\
&\left\langle Q+1, S_z-\tfrac{1}{2}, r, 3\right|P^\dagger_{N\downarrow}|Q, S_z, r, 1\rangle_N = 1,\\
&\left\langle Q+1, S_z-\tfrac{1}{2}, r, 4\right|P^\dagger_{N\downarrow}|Q, S_z, r, 2\rangle_N = -1.
\end{aligned} \tag{36}$$

Clearly, to get $\langle Q, S_z, r|P^\dagger_{N\sigma}|Q', S'_z, r'\rangle_N$, we need the transformation matrix $U_N(Q, S_z, r, w, i)$ that diagonalizes the block in H_N labeled by Q and S_z. In other words, $U_N(Q, S_z, r, w, i)$ connects the energy eigenstate $|Q, S_z, r\rangle_N$ with the basis states $|Q, S_z, w, i\rangle_N$ by

$$|Q, S_z, r\rangle_N = U_N(Q, S_z, r, w, i)|Q, S_z, w, i\rangle_N. \tag{37}$$

Here both r and w label the ordering of the state and $i = 1$–4 with labels 1, 2, 3, and 4 representing the N state for adding a holon, one spin-up particle, one spin-down particle, and two particles to $N-1$ state as we go from $N-1$ to N states. Using $U_N(Q, S_z, r, w, i)$, one can compute $\langle Q, S_z, r|P^\dagger_{N\sigma}|Q', S'_z, r'\rangle_N$.

As a example, consider the computation of $\langle q, r, 1|H^I_{N,1}|q, r', 2\rangle_{N+1}$, which can be reduced to matrix element of $P^\dagger_{N\uparrow}$ in the energy eigenstates as $\langle Q+1, S_z, r|P^\dagger_{N\uparrow}|Q, S_z-\frac{1}{2}, r'\rangle_N$. By using Eq. (37), one can express $|Q, S_z-\frac{1}{2}, r'\rangle_N$ in terms of $|Q, S_z-\frac{1}{2}, r', w, 1\rangle_{N-1}$ or $|Q, S_z-\frac{1}{2}, r', w, 3\rangle_{N-1}$. Similarly, $|Q+1, S_z, r\rangle_N$ can be expressed in terms of $|Q+1, S_z, r, w, 2\rangle_{N-1}$ or $|Q+1, S_z, r, w, 4\rangle_{N-1}$. We find

$$\begin{aligned}
&\langle q, r, 1|H^I_{N,1}|q, r', 2\rangle_{N+1}\\
&\quad= U^*_N(Q+1, S_z, r, w, 2)U_N\left(Q, S_z-\tfrac{1}{2}, r', w, 1\right)\\
&\qquad+U^*_N(Q+1, S_z, r, w, 4)U_N\left(Q, S_z-\tfrac{1}{2}, r', w, 3\right).
\end{aligned}$$

Similarly, we can find all other matrix elements.

Similarly, the nonvanishing matrix elements of hopping Hamiltonian $H^I_{N,2} = \sum_\sigma P^\dagger_{N\sigma}P_{N+2\sigma} + \text{H.c.}$ can be obtained as

$$\begin{aligned}
H^{I,(q,1,2)_{N+2}}_{N,2} &= \langle Q+1, S_z, r|P^\dagger_{N\uparrow}\left|Q, S_z-\tfrac{1}{2}, r'\right\rangle_{N+1},\\
H^{I,(q,3,4)_{N+2}}_{N,2} &= -\left\langle Q, S_z+\tfrac{1}{2}, r\right|P^\dagger_{N\uparrow}|Q-1, S_z, r'\rangle_{N+1},\\
H^{I,(q,1,3)_{N+2}}_{N,2} &= \langle Q+1, S_z, r|P^\dagger_{N\downarrow}\left|Q, S_z+\tfrac{1}{2}, r'\right\rangle_{N+1},\\
H^{I,(q,2,4)_{N+2}}_{N,2} &= \left\langle Q, S_z-\tfrac{1}{2}, r\right|P^\dagger_{N\downarrow}|Q-1, S_z, r'\rangle_{N+1},
\end{aligned} \tag{38}$$

where $H^{I,(q,i,j)_{N+2}}_{N,2}$ is a shorthand symbol for $\langle q, r, i|H^I_{N,2}|q, r', j\rangle_{N+2}$.

Similar construction shows that the nonvanishing matrix elements of $P^\dagger_{N\sigma}$ in basis states with $N+1$ sites are given by

$$\begin{aligned}
\langle q, r, 1|P^\dagger_{N\sigma}|q', r', 1\rangle_{N+1} &= \langle Q+1, S_z, r|P^\dagger_{N\sigma}|Q'+1, S'_z, r'\rangle_N,\\
\langle q, r, 2|P^\dagger_{N\sigma}|q', r', 2\rangle_{N+1} &= -\left\langle Q, S_z-\tfrac{1}{2}, r\right|P^\dagger_{N\sigma}\left|Q', S'_z-\tfrac{1}{2}, r'\right\rangle_N,\\
\langle q, r, 3|P^\dagger_{N\sigma}|q', r', 3\rangle_{N+1} &= -\left\langle Q, S_z+\tfrac{1}{2}, r\right|P^\dagger_{N\sigma}\left|Q', S'_z+\tfrac{1}{2}, r'\right\rangle_N,\\
\langle q, r, 4|P^\dagger_{N\sigma}|q', r', 4\rangle_{N+1} &= \langle Q-1, S_z, r|P^\dagger_{N\sigma}|Q'-1, S'_z, r'\rangle_N.
\end{aligned} \tag{39}$$

One can thus obtain $\langle Q, S_z, r|P^\dagger_{N\sigma}|Q', S'_z, r'\rangle_{N+1}$ by using $U_{N+1}(Q, S_z, r, w, i)$, $U_N(Q, S_z, r, w, i)$, Eq. (36), and Eq. (39). Note that the above procedure can be easily generalized to the hopping Hamiltonian $\sum_\sigma P^\dagger_{N\sigma}P_{N+l\sigma} + \text{H.c.}$ for arbitrary number l.

2. *Iterative diagonalization in (Q, S_z, P) basis*

Let $|Q, S_z, P, r\rangle_N$ denote the eigenstates of H_N, i.e.,

$$H_N|Q, S_z, P, r\rangle_N = E_N(Q, S_z, P, r)|Q, S_z, P, r\rangle_N, \tag{40}$$

where $P = \pm 1$ labels the parity of states.

The basis states for new states when adding new site fermions $P^\dagger_{N+1\sigma}$ depend on whether N is even or odd. For N even, basis states are given by

$$\begin{aligned}
|q, r, 1\rangle_{N+1} &= |0; Q+1, S_z, r\rangle_N,\\
|q, r, 2\rangle_{N+1} &= \left|\uparrow_{N+1}; Q, S_z-\tfrac{1}{2}, P, r\right\rangle_N,\\
|q, r, 3\rangle_{N+1} &= \left|\downarrow_{N+1}; Q, S_z+\tfrac{1}{2}, P, r\right\rangle_N,\\
|q, r, 4\rangle_{N+1} &= |\uparrow\downarrow_{N+1}; Q-1, S_z, P, r\rangle_N,
\end{aligned} \tag{41}$$

while for N odd, basis states are given by

$$\begin{aligned}
|q, r, 1\rangle_{N+1} &= |0; Q+1, S_z, r\rangle_N,\\
|q, r, 2\rangle_{N+1} &= \left|\uparrow_{N+1}; Q, S_z-\tfrac{1}{2}, -P, r\right\rangle_N,\\
|q, r, 3\rangle_{N+1} &= \left|\downarrow_{N+1}; Q, S_z+\tfrac{1}{2}, -P, r\right\rangle_N,\\
|q, r, 4\rangle_{N+1} &= |\uparrow\downarrow_{N+1}; Q-1, S_z, P, r\rangle_N,
\end{aligned} \tag{42}$$

where q is the shorthand of $(Q+1, S_z, P)$. Note that the parity of any many-particle state changes sign when adding an odd number of fermions, while the parity stays the same when adding an even number of fermions.

Note that to preserve the parity, the hopping Hamiltonian now only includes $H^I_{N,2} = \sum_\sigma P^\dagger_{N\sigma} P_{N+2\sigma} + \text{H.c.}$ terms, whose nonvanishing matrix elements are given by

$$\begin{aligned}
H^{I,(q,1,2)_{N+2}}_{N,2} &= \langle Q+1, S_z, P, r|P^\dagger_{N\uparrow}|Q, S_z-\tfrac{1}{2}, (-1)^{N+1}P, r'\rangle_{N+1},\\
H^{I,(q,3,4)_{N+2}}_{N,2} &= -\langle Q, S_z+\tfrac{1}{2}, (-1)^{N+1}P, r|P^\dagger_{N\uparrow}|Q-1, S_z, P, r'\rangle_{N+1},\\
H^{I,(q,1,3)_{N+2}}_{N,2} &= \langle Q+1, S_z, P, r|P^\dagger_{N\downarrow}|Q, S_z+\tfrac{1}{2}, (-1)^{N+1}P, r'\rangle_{N+1},\\
H^{I,(q,2,4)_{N+2}}_{N,2} &= \langle Q, S_z-\tfrac{1}{2}, (-1)^{N+1}P, r|P^\dagger_{N\downarrow}|Q-1, S_z, P, r'\rangle_{N+1}.
\end{aligned} \tag{43}$$

The remaining steps for computing the matrix elements $\langle Q, S_z, P, r|P^\dagger_{N\sigma}|Q', S'_z, P, r'\rangle_N$ are the same as what were done for basis states using (Q, S_z). Here, relevant identities, similar to Eqs. (36), are given by

$$\begin{aligned}
&\langle Q+1, S_z+\tfrac{1}{2}, P^*, w, 2|P^\dagger_{N\uparrow}|Q, S_z, P, w, 1\rangle_N = 1,\\
&\langle Q+1, S_z+\tfrac{1}{2}, P^*, w, 4|P^\dagger_{N\uparrow}|Q, S_z, P, w, 3\rangle_N = 1,\\
&\langle Q+1, S_z-\tfrac{1}{2}, P^*, w, 3|P^\dagger_{N\downarrow}|Q, S_z, P, w, 1\rangle_N = 1,\\
&\langle Q+1, S_z-\tfrac{1}{2}, P^*, w, 4|P^\dagger_{N\downarrow}|Q, S_z, P, w, 2\rangle_N = -1,
\end{aligned} \tag{44}$$

where $P^* = (-1)^{N+1}P$, and relevant matrix elements are given by

$$\begin{aligned}
&\langle q, r, 1|P^\dagger_{N\sigma}|q', r', 1\rangle_{N+1}\\
&\quad = \langle Q+1, S_z, P, r|P^\dagger_{N\sigma}|Q'+1, S'_z, P', r'\rangle_N,
\end{aligned} \tag{45}$$

$$\begin{aligned}
&\langle q, r, 2|P^\dagger_{N\sigma}|q', r'2\rangle_{N+1}\\
&\quad = -\langle Q, S_z-\tfrac{1}{2}, P, r|P^\dagger_{N\sigma}|Q', S'_z-\tfrac{1}{2}, P', r'\rangle_N,\\
&\langle q, r, 3|P^\dagger_{N\sigma}|q', r'3\rangle_{N+1}\\
&\quad = -\langle Q, S_z+\tfrac{1}{2}, P, r|P^\dagger_{N\sigma}|Q', S'_z+\tfrac{1}{2}, P,' r'\rangle_N,\\
&\langle q, r, 4|P^\dagger_{N\sigma}|q', r', 4\rangle_{N+1}\\
&\quad = \langle Q-1, S_z, r|P^\dagger_{N\sigma}, P|Q'-1, S'_z, P', r'\rangle_N.
\end{aligned} \tag{46}$$

D. Numerical iterative diagonalization and error analysis

Based on the effective 1D chain Hamiltonian, one can perform the iterative diagonalization procedure by diagonalizing H^W_1 and H^W_2 iteratively [24,27,28]. Here, eigenstates of the 1D chain Hamiltonian H^W_1 are classified by the quantum number, charge Q, z component of total spin S_z, and additional parity number P in H^W_2. In the iterative diagonalization, one derives matrix elements of the effective 1D chain Hamiltonian of $N+1$ sites (single impurity) or $N+2$ sites (two impurities) from eigenstates of N sites [26]. The resulting effective 1D chain Hamiltonian of $N+1$ sites (single impurity) or $N+2$ sites are then exactly diagonalized. For each iteration step, numbers of eigenstates kept are $N_{tr} = 10\,000$ for the single-impurity and $N_{tr} = 6000$ for the two-impurities case. By comparing with the exact excitation energies when $\Gamma = 0$, the relative error of our calculations at $k_BT \ll \varepsilon_B$ can be estimated to be less than 0.01% for the single impurity and less than 1% for two impurities.

Note that in typical research on Kondo effects, the impurity is embedded in a continuous conduction band. The main difficulty in typical Kondo problem arises from infinite degrees of freedom for excitation energies lower than any given finite temperature T. Therefore, the suitable approximated NRG Hamiltonian in wild-temperature range to zero-temperature limit is required. This gives the requirement of the exponentially decayed t_m by the perturbation argument in Wilson's original NRG paper.

However, in our considered situation, which is primarily at zero temperature, the system is under strong magnetic field and is at temperature T much lower than the Landau-level energy spacing ε_B. Only a small number ($N_t < 20$) of Landau levels is within the energy cutoff D. Therefore, below our interested temperature, only few degrees of freedom for excitation energies are allowed. Although t_m does not decay exponentially, for small N_t and a large number of kept states in each iteration, the iterative diagonalization procedure still provides low-energy excitations and states with high accuracy. In particular, we find that our results converge as N_t increases. This indicates that the energy scale of high- and low-energy modes separates in our approach. Furthermore, we find that t_m follows a scaling form $t_m/D = f(m/N_t)$ with $f(x)$ being roughly in the form of $a - bx^2$. The existence of this scaling form implies that there is a finite-size rescaling involved when one goes from one scale to another, indicating the close relation of our method to the renormalization group analysis.

IV. PHASES OF MANY-BODY GROUND STATE

In this section, we will describe the emergent phases in the many-body ground state. Before we describe these phases, we shall first examine the application regime of our calculations. In our iterative diagonalization procedure, there are N_t Landau levels with discrete energies within the cutoff D. For a given temperature T, there are two regimes: (1) Regime of weak magnetic fields in which $\varepsilon_B \ll k_BT \ll D$ so that N_t is essentially infinite and the number of Landau levels below k_BT is also essentially infinite. This is the regime that one may apply the Wilsons discretization scheme. (2) Regime of strong magnetic fields in which there are a finite number N_t of Landau levels within the cutoff D. For typical strong magnetic fields around 10 T, N_t is the order of 10 to 10^2. This is the situation concerned in our NRG scheme. In this regime, one needs to consider Kondo effects from a finite number of Landau levels. Furthermore, because our iterative diagonalization procedure is accurate for low-energy excitations, it further sets a limit that the temperature is much lower than the Landau-level energy spacing ε_B, i.e., $k_BT < \varepsilon_B$. From the view of renormalization group method, the system is finite and one

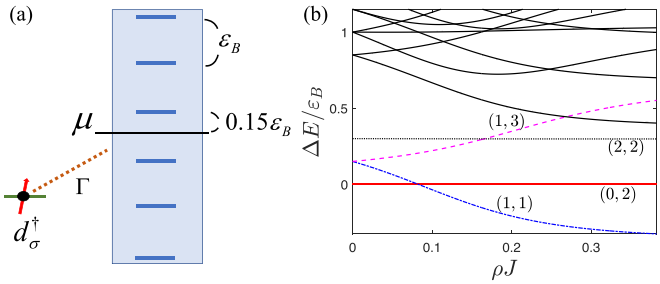

FIG. 4. (a) Schematic diagram for single-impurity coupling to Landau levels within the cutoff D (shaded area). (b) Many-particle eigenenergy difference $E(Q, 2S+1, r) - E(0, 2, r_{\min})$, obtained from the iterative diagonalization method, where numbers shown in brackets label $(Q, 2S+1)$ and $\rho J = \frac{\Gamma}{\pi}(\frac{1}{|U+\xi_d|} + \frac{1}{|\xi_d|})$.

can not perform infinite iterations and go to the fixed point. Instead, as it is well known, there will be finite-size effects and one needs to do finite-size scaling to get results for infinite systems. This is particularly true for scaling functions and scaling exponents. In this work, however, we are interested in phases of the ground states. Therefore, the finite-size effect is not particularly important as one will see in the following that changes of N_t have limited effects.

A. Transition between doublet and singlet ground states and the phase diagram when $g_c = g_d = 0$

To realize how the Kondo physics affects the many-body ground state, we start with the single-impurity case when $g_c = g_d = 0$. In this case, the Hamiltonian possesses additional SU(2) symmetry of total spin, which allows us to classify eigenstates by total spin S [27,28], which provides more accurate description of states and excitation energy. Therefore, we shall label states by using quantum numbers Q and S and denote eigenstates by $|Q, 2S+1, r\rangle$ and energy eigenvalues by $E(Q, 2S+1, r)$.

When $\Gamma = 0$, the ground state is $|0, 2, r_{\min}\rangle$, where the labeling $r_{\min}$ is used to indicate that the energy of the ground state is the minimum of all $|0, 2, r\rangle$. The state $|0, 2, r_{\min}\rangle$ is doubly degenerated and will persist to be an eigenstate but may not be the ground state when $\Gamma \neq 0$. In Fig. 4(a), we show the coupling of the impurity to Landau levels schematically. Here even the number of Landau quantized bands in the energy cutoff D is shown. The chemical potential is set in the central two Landau levels, and below the upper level with $0.15\varepsilon_B$. In Fig. 4(b), we show the energy difference ΔE between first few low-energy states and doublet states $|0, 2, r_{\min}\rangle$ at different ρJ. Here in the calculations, we change the parameter Γ but in the plot shown in Fig. 4(b), we use ρJ as the variable for the x axis. ρJ is related to Γ by [1]

$$\rho J = \frac{\Gamma}{\pi}\left(\frac{1}{|U+\xi_d|} + \frac{1}{|\xi_d|}\right). \tag{47}$$

For each given Γ, from numerical calculation, one obtains low-energy states $|Q, 2S+1, r\rangle$ and spectrum $E(Q, 2S+1, r)$ classified by the quantum number $(Q, 2S+1)$. To make the competition between two ground states more clear, the energy difference ΔE is taken as $E(Q, 2S+1, r) - E(0, 2, r_{\min})$ as shown in Fig. 4.

Let us first examine low-energy many-body states at $\Gamma = 0$ as shown in Fig. 4(b). When $\Gamma = 0$, the ground state $|E_0(\Gamma = 0)\rangle$ of the system is the direct product of the ground state for the impurity ground state $|E_0^d(\Gamma = 0)\rangle$ and the ground state of conduction electrons $|E_0^c(\Gamma = 0)\rangle$. Here, the ground state of the conduction electrons $|E_0^c(\Gamma = 0)\rangle$ is the state with all levels below μ being doubly occupied. For $\xi^d < 0$ and $U + \xi^d > 0$, the impurity prefers singly occupied and hence the ground state of the spin is doubly degenerated due to spin. As a result, the ground state $|E_0(\Gamma = 0)\rangle$ possesses $Q = 0$ and degeneracy $2S + 1 = 2$. The first excited state $|E_1(\Gamma = 0)\rangle$ has four degeneracies. This corresponds to the addition of a charge into the ground state of the conduction electrons (so its $Q = 1$) with energy $0.15\varepsilon_B$, and the degeneracy 4 comes from the spin of impurity and the spin of added charge. The second excited state $|E_2(\Gamma = 0)\rangle$ has two degeneracies, which correspond to the addition of two charges into the ground state of the conduction electrons with total energy $0.3\varepsilon_B$. The degeneracy comes from the spin of the impurity.

When Γ is turned on, the Kondo spin-spin interaction starts to show up between the impurity and conduction electron. However, many-particle states of conduction electrons must carry spins so that it can screen the spin of the impurity. Therefore, as shown in Fig. 4(b), the competition between single-charge excitation energy $(0.15\varepsilon_B)$ at $\Gamma = 0$ and the Kondo interaction energy when Γ is finite results in the quantum phase transition between the local moment doublet and Kondo singlet state, as displayed in the crossover between the red solid line and blue dashed-dotted line. In addition, spin-triplet states are shown in pink dashed line where its energy increases when Γ increases as predicted by the sign of Kondo interaction. Furthermore, we notice that the energy difference between $|E_0(\Gamma = 0)\rangle$ and $|E_2(\Gamma = 0)\rangle$ is almost unchanged when Γ increases to large values, which also agrees with the argument that the Kondo interaction only significantly affects many particles of conduction electrons.

Based on the degeneracy of ground state at different μ and Γ, we plot the phase diagram in the parameter space of μ and ρJ in Figs. 5(a) and 5(b), where for doublet phase $(2S + 1 = 2)$ we denote it as Un (unscreened) phase and for singlet phase $(2S + 1 = 1)$ we denote it as Sc (screened) phase. The Kondo screening feature in these phases can be checked by examining the spin-spin correlation $\langle \vec{s}_d \cdot \vec{s}_{f_1} \rangle$ between the impurity d and the first site f_1 of the 1D chain. This is shown in Figs. 5(c) and 5(d), in which we see that in agreement with the Kondo screening feature, the spin-spin correlation is negatively enhanced when the system enters into the screened phase.

B. Phase diagram and magnetic moment when $g_c \neq 0$ and $g_d \neq 0$

When $g_c \neq 0$ and $g_d \neq 0$, the Zeeman splitting term in the Hamiltonian generally breaks the typical temperature-driven Kondo effect in weak fields [29]. To simplify the numerical calculation, we define new $\tilde{g}$ factors as

$$\tilde{g}_c = g_c \frac{\mu_B B}{\varepsilon_B}, \quad \tilde{g}_d = g_d \frac{\mu_B B}{\varepsilon_B}. \tag{48}$$

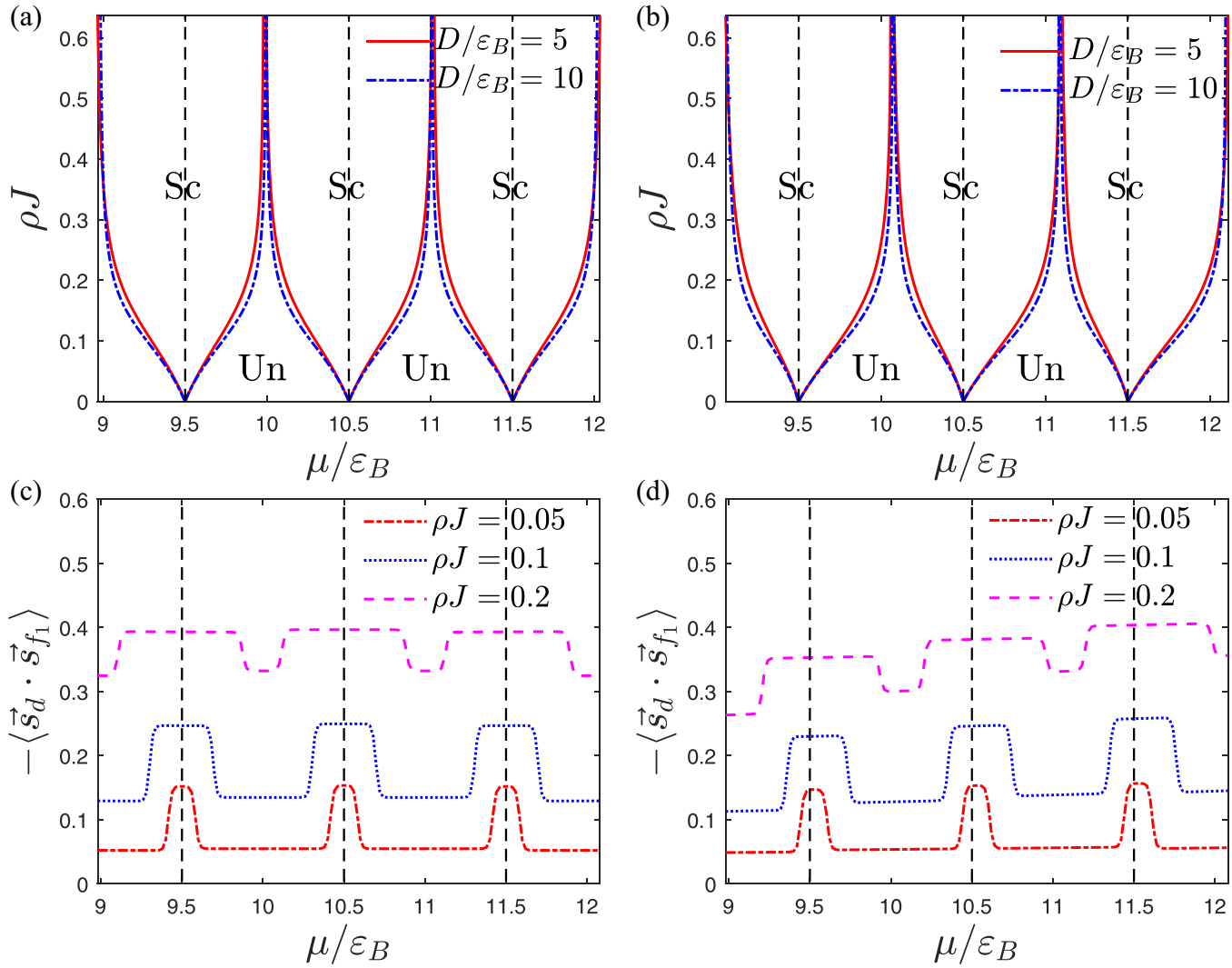

FIG. 5. Phase diagram of many-body ground states in the absence of Zeeman splitting. Here states are classified by degeneracy $2S+1$. For $2S+1=1$ phase is denoted as Sc (screened), for $2S+1=2$ phase is denoted as Un (unscreened). Here $\rho J = \frac{\Gamma}{\pi}(\frac{1}{|U+\xi_d|} + \frac{1}{|\xi_d|})$, and $\xi_d = -5D$. The vertical black dashed line marks the position of Landau level before hybridization. (a) $U = 10D$, the impurity Hamiltonian possesses particle-hole symmetry. (b) $U = 10^4 D$, this is the typical infinite-U region, which can be described by the $t-J$ model. (c) $U = 10D$, quantum oscillation of spin-spin correlation strength $\langle \vec{s}_d \cdot \vec{s}_{f_1} \rangle$, which is negatively enhanced when the system enters into the screened phase. (d) $U = 10^4 D$.

Note that when the effective electron mass m_e^* is equal to the free-electron mass, one has $\tilde{g}_c = g_c$ and $\tilde{g}_d = g_d$.

Since $g_c \neq 0$ and $g_d \neq 0$, the total spin S is not a good quantum number. Therefore, phase diagram at zero temperature is obtained by keeping track of change of the quantum numbers S_z in the lowest-energy state. From S_z (the z component of total spin) of the lowest energy state at $\rho J = 0$ and finite ρJ, one obtains change of S_z that is due to the Kondo interaction as

$$\Delta S_z \equiv S_z^0(\rho J) - S_z^0(\rho J = 0), \tag{49}$$

where the superscript 0 indicates that S_z^0 is S_z of the ground state. Using ΔS_z, we identify phases of the system as shown in Figs. 6(a), 6(b), 7(a), and 7(b). Note that the system is composed by electrons and hence possible values of total spin are half-integers, i.e., $S = 0, \frac{1}{2}, 1, \frac{3}{2}, \ldots$. Hence, possible values of ΔS_z are $0, \pm\frac{1}{2}, \pm 1, \ldots$.

When $\tilde{g}_d > 0$, $\tilde{g}_c > 0$, and $\rho J = 0$, $S_z^{\rm imp}$ of the impurity in ground state is $-\frac{1}{2}$; while S_z^c of conduction electrons can be $-\frac{1}{2}$ or 0, depending on whether the chemical potential lies between two Zeeman-split Landau levels or not. Therefore, total S_z at $\rho J = 0$ is equal to -1 or $-\frac{1}{2}$, i.e., $S_z^0(\rho J = 0) = -1$ or $-\frac{1}{2}$. When $\rho J > 0$, $S_z^{\rm imp}$ can be screened or unscreened. Clearly, if $S_z^{\rm imp}$ is unscreened, we have $\Delta S_z = 0$. This is the situation when $S_z^{\rm imp} = -\frac{1}{2}$ and $S_z^c = 0$ as conduction electrons have no spin to screen the impurity. In general, finite $\langle S_z^{\rm imp} \rangle < 0$ of the impurity together with the Kondo interaction generates an effective negative g factor $J\langle S_z^{\rm imp} \rangle S_z^c$. This changes S_z^c of conduction electrons from $-\frac{1}{2}$ to 0 or $\frac{1}{2}$, which corresponds to $\Delta S_z = \frac{1}{2}$ or $\Delta S_z = 1$, respectively, which is consistent with

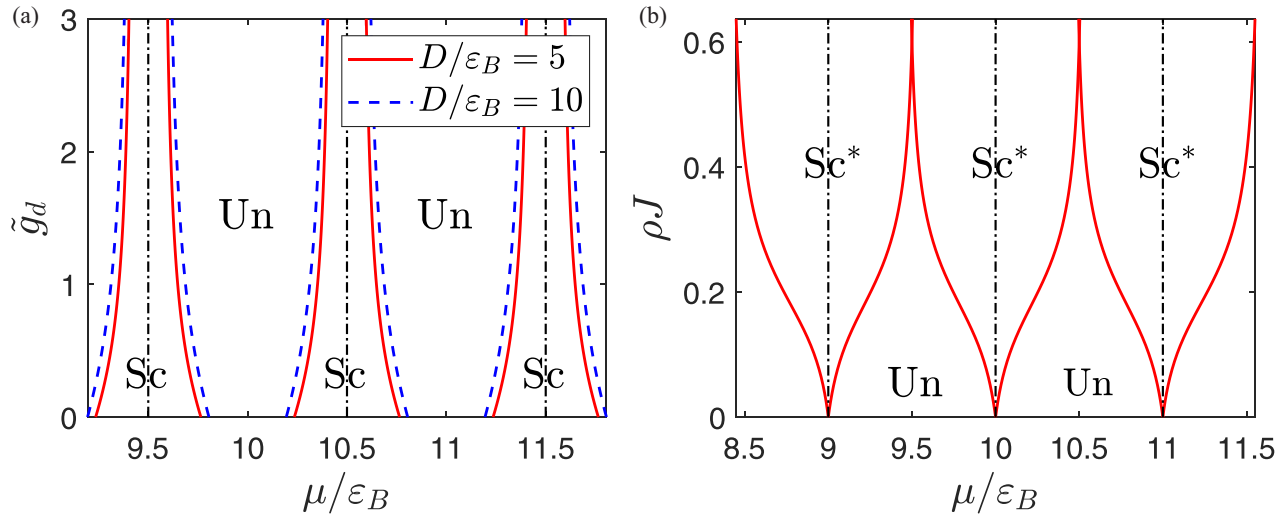

FIG. 6. Phase diagram of many-body ground states in the presence of Zeeman splitting. Here states are classified by $\Delta S_z \equiv S_z^0(\rho J) - S_z^0(\rho J = 0)$. "Sc" denotes the Kondo screening state with $\Delta S_z = \frac{1}{2}$, "Sc*" denote the Kondo screening state with $\Delta S_z = 1$, and "Un" denotes the unscreened impurity state. The parameter is taken as $\rho J = \frac{\Gamma}{\pi}(\frac{1}{|U+\xi_d|} + \frac{1}{|\xi_d|})$, $U = 10D$, $\xi_d = -5D$. The vertical black dashed line marks the position of Landau level before hybridization. (a) $\tilde{g}_c = 0$, $\rho J = 0.127$. (b) $\tilde{g}_c = \tilde{g}_d = 2$, $D/\varepsilon_B = 10$.

ΔS_z anticipated for half-integer systems. Thus, by exploring ΔS_z, we obtain unscreened phases with $\Delta S_z = 0$, and the Kondo screening state with $\Delta S_z = \frac{1}{2}$ and $\Delta S_z = 1$ labeled by Sc and Sc*, respectively. In the Sc* phase, both the impurity spin and spin of conduction electrons vanishes due to Kondo screening. Clearly, as shown in Figs. 6(a), 6(b), 7(a), and 7(b), phases of the ground state oscillate among "Sc," "Un," and "Sc*" states as the chemical potential μ changes.

This results in quantum oscillations in magnetic moments as shown in Figs. 7(c) and 7(d). Here the total magnetic moment $M_{\rm tot}$ is computed by the definition $M_{\rm tot} = -\frac{\partial\Omega}{\partial B}$, where $\Omega = -\frac{1}{\beta}{\rm Tr}(e^{-\beta H})$ [30] and can be decomposed as the summation of the magnetic momentums due to the orbit moment of conduction electrons M_c, the hybridization part $M_{\rm hyb}$, the spin moment of conduction electrons $M_{c,s}$, the spin moment of the impurity $M_{d,s}$. The detail of each parts is as follows:

$$\begin{aligned} M_c &= -2\mu_B \sum_{\{n\},\sigma} \left(n + \frac{1}{2}\right) \langle A^\dagger_{n\sigma} A_{n\sigma}\rangle, \\ M_{\rm hyb} &= -\mu_B (\Gamma/\pi\varepsilon_B)^{1/2} \sum_{\{n\},\sigma} \langle d^\dagger_\sigma A_{n\sigma} + {\rm H.c.}\rangle, \\ M_{c,s} &= -\frac{\mu_B g_c}{2} \sum_{\{n\}} \langle A^\dagger_{n\uparrow} A_{n\uparrow} - A^\dagger_{n\downarrow} A_{n\downarrow}\rangle, \\ M_{d,s} &= -\frac{\mu_B g_d}{2} \langle d^\dagger_\uparrow d_\uparrow - d^\dagger_\downarrow d_\downarrow\rangle. \end{aligned} \tag{50}$$

Note that we only keep one channel in the Landau level that couples to the impurity in H_1 and the remaining $N_L - 1$ channels are disregarded [cf. Eq. (13)]. Hence, for dilute impurity systems with impurity number being $N_{\rm imp}$, the moment of total system is given by $(N_L - N_{\rm imp})(M_c^0 + M_{c,s}^0) + N_{\rm imp} M_{\rm tot} = N_L(M_c^0 + M_{c,s}^0) + N_{\rm imp} M_{d,s}^0 + N_{\rm imp}(M_{\rm tot} - M_{\rm tot}^0)$, where M_c^0 and $M_{c,s}^0$ are magnetic moments due to the orbit and spin of conduction electrons in the absence of hybridization, $\Gamma = 0$. The total magnetic moment induced by impurity, shown in Fig. 7(d), is then given by $M_{\rm ind}^{\rm imp} = M_{\rm tot} - M_{\rm tot}^0$, where the magnetic moment with the superscript 0 denotes the same moment when $\Gamma = 0$. The total moment of Kondo system with dilute impurities in strong fields is equal to

$$M = M_0 + N_{\rm imp} M_{\rm imp} + N_{\rm imp} M_{\rm ind}^{\rm imp}, \tag{51}$$

where M_0 is the moment of pure Landau quantized system, $M_{\rm imp}$ is the single-impurity moment equal to $g_d \mu_B$ at low temperature, and $M_{\rm ind}^{\rm imp}$ is the induced moment by impurity.

We now explore two Kondo impurities in the presence of strong magnetic fields. In Fig. 8, we show results of numerical iterative diagonalization on allowed phases of the system for different density of states. For two impurities in strong magnetic fields, we find that the interplay between the Kondo screening effect, RKKY interaction, and quantum oscillations due to Landau levels determines the ground state of the system. Specifically, the combination of these factors results in different screening scenarios for different phases as shown in Fig. 8(c). Here as determined by RKKY interaction, spins of two impurities marked by red color may form a singlet state, triplet state, or two independent spin-$\frac{1}{2}$ states. The impurity spins then get screened by conduction electrons marked by blue color. As a result, as shown in Fig. 8(c), we find that ground states can be an unscreened triplet state, unscreened singlet state, partial screened triplet state, partial screened singlet state, and two screened spin-$\frac{1}{2}$ states. These states are characterized by different quantum number S_z's that reflect the scenario such that the corresponding $S_z = 1$, 0, $\frac{1}{2}$, $\frac{1}{2}$, and 0. Furthermore, states shown in Fig. 8(c) form different phases so that the ground state of the system with Kondo impurities oscillates between these states when either the magnetic field or the distance between Kondo impurities changes as shown in Figs. 8(a) and 8(b). This oscillation leads to quantum oscillation in magnetization and conductivities as shown in Fig. 9.

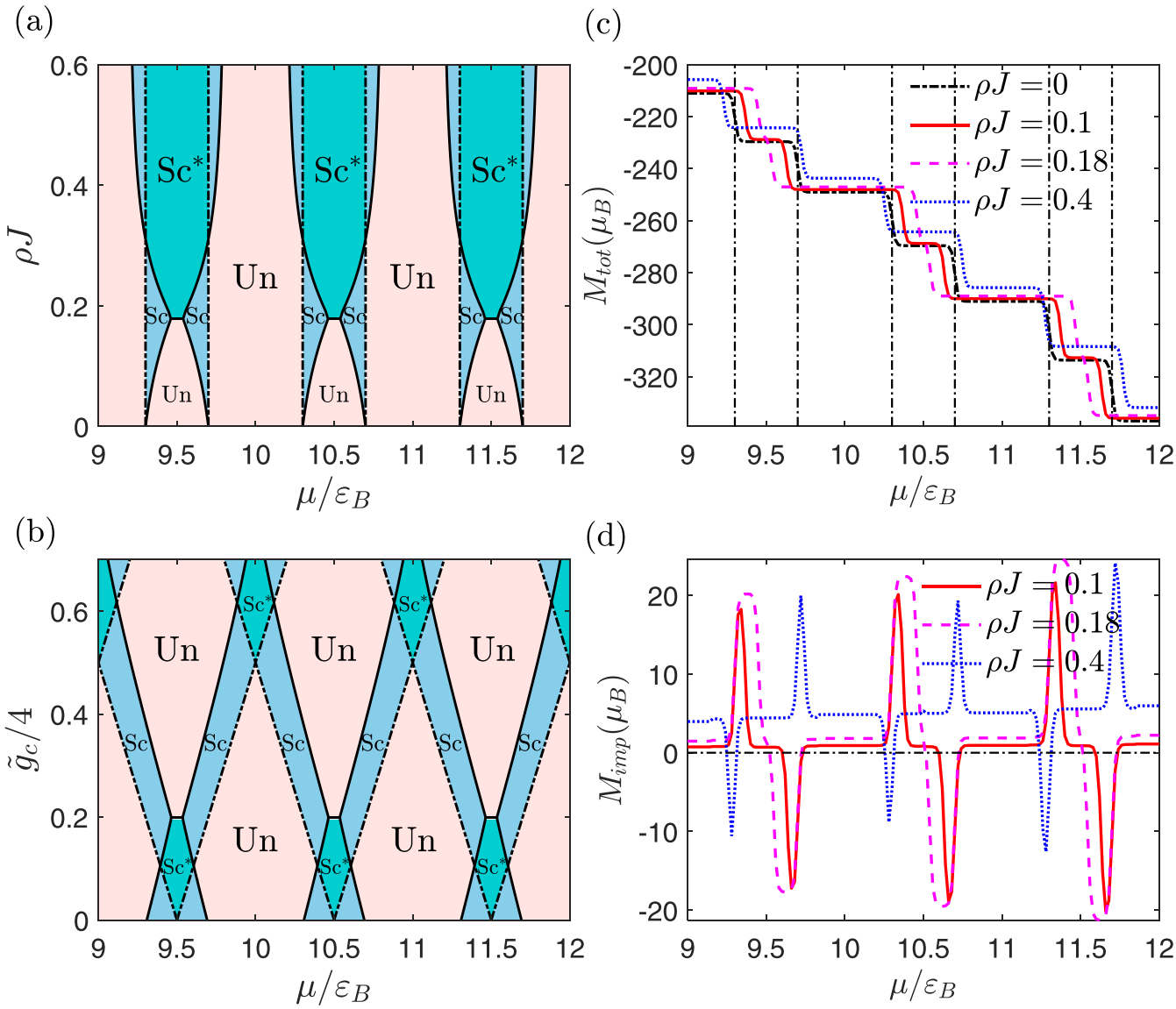

FIG. 7. (a) Phase diagram of single Kondo impurity in the parameter space ρJ versus chemical potential μ. Here $g_c = 0.8$, $g_d = 2$, "Sc" denotes the Kondo screening state with $\Delta S_z = \frac{1}{2}$, "Sc*" denotes the Kondo screening state with $\Delta S_z = 1$, and "Un" denotes the unscreened impurity state. (b) Phase diagram of single Kondo impurity in the parameter space g_c versus chemical potential. Here g_d is fixed at 2. (c) Quantum oscillation in total magnetic moment at temperature $k_BT/D = 0.005$ (sum of magnetic moments of the Kondo impurity and the conduction electrons, see text for definition), the vertical black dashed line marks the position of split Landau level before hybridization is turned on. (d) Quantum oscillation of the total magnetic moment induced by impurity. Here parameters are $\varepsilon_B/D = 0.2$, $U/D = 10$, $\xi_d/D = -5$, and $\rho J = \frac{\Gamma}{\pi}(\frac{1}{|U+\xi_d|} + \frac{1}{|\xi_d|})$.

Here the longitudinal conductivity σ_{xx} and Hall conductivity σ_{xy} are computed by

$$\sigma^{xx} = \sum_s \sigma_s^{xx},$$

$$\sigma_s^{xx} = \frac{e^2\varepsilon_B^2}{2\pi^2\hbar}\int dE\ \frac{-\partial f(E)}{\partial E} \times \sum_n (n+1)\mathrm{Im}G^c_{n,s}(E+i\delta)\mathrm{Im}G^c_{n+1,s}(E+i\delta), \quad (52)$$

$$\Delta\sigma^{xy} = \sum_s -2\frac{\mathrm{Im}\Sigma_s(0+i\delta)}{\varepsilon_B}\sigma_s^{xx}. \quad (53)$$

Here s labels the spin of conduction electrons, $f(E) = 1/(1 + e^{E/k_BT})$ is the Fermi-Dirac function [31], and $G^c_{n,s}(E) = \langle G^c_{n,k_y,s}(E)\rangle$ is the renormalized Green's function for conduction electrons with the average over all Landau degeneracies k_y of nth Landau level being taken. In terms of the self-energy $\Sigma_{n,k_y,s}$, $G^c_{n,k_y,s}(E)$ can be expressed as

$$G^c_{n,k_y,s}(E) = \frac{1}{E - (n+1/2+s)\varepsilon_B - \Sigma_{n,k_y,s}}. \quad (54)$$

Here the contribution to the self-energy comes from the scattering of the conduction electrons by magnetic impurities. At low impurity density, this self-energy $\Sigma_{n,k_y,s}$ can

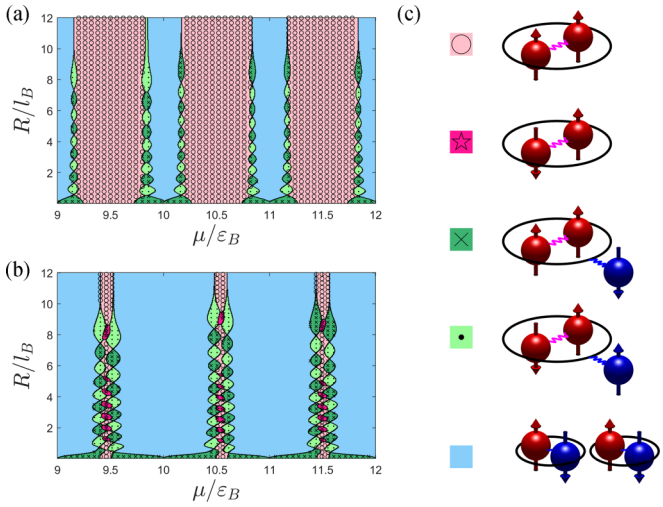

FIG. 8. Phase diagram of two Kondo impurities in strong magnetic fields for (a) $\rho J = 0.18$ and (b) $\rho J = 0.45$. (c) Different screening scenarios of two Kondo impurities in phases shown in (a) and (b). Here parameters used are $g_c = g_d = 2$, $\varepsilon_B/D = \frac{1}{3}$, $U/D = 10$, and $\xi_d/D = -5$. As determined by RKKY interaction, spins of two impurities marked by red color may form singlet state, triplet state, or two independent spin-$\frac{1}{2}$ states. The impurity spins then get screened by conduction electrons marked by blue color.

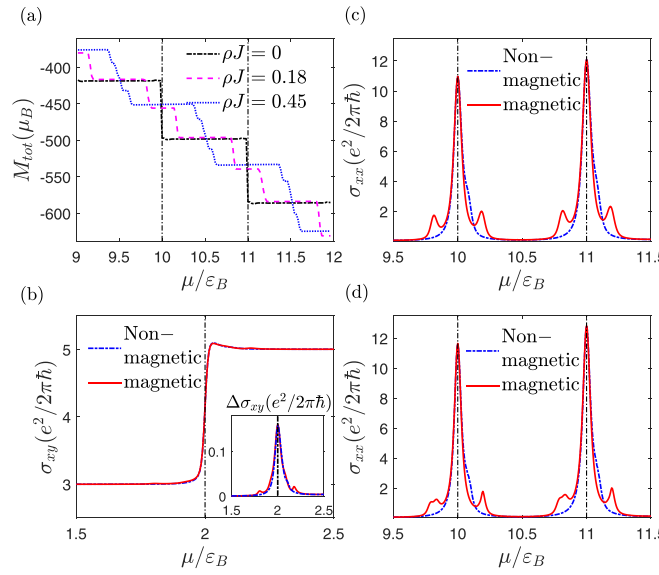

FIG. 9. Quantum oscillation exhibited in two Kondo impurities under strong magnetic field. (a) Total magnetization versus the chemical potential (μ) in unit of ε_B. Comparison of contribution of nonmagnetic and magnetic impurities to Hall conductivity (b) and longitudinal conductivity (c) for one impurity. (d) Same comparison of two impurities for longitudinal conductivity. Here side peaks are due to extra density of states released from total screened state to partial screened or unscreened states (see text). Parameters used are $\varepsilon_B/D = \frac{1}{3}$, $U/D = 10$, $\xi_d/D = -5$, $\rho J = 0.18$, $B = 10$ T, $k_BT/D = 0.005$, $R/l_B = 216$ nm, and the effective impurity scattering constant is $w_{\rm imp} = 0.0025$ (see [26]).

be expanded in terms of the impurity density $O(n_{\rm imp})$. For the single-impurity case, $\Sigma_{n,k_y,s} = n_{\rm imp}\Gamma/(\pi\rho)G_s^d$, while for the two-impurities case, $\Sigma_{n,k_y,s} = n_{\rm imp}\Gamma/(\pi\rho)(G_{11,s}^d + G_{22,s}^d)$. Here G_s^d generally represents the Green's function for electrons of the impurities, i.e., the d electrons. The one-impurity Green's function is represented by G_s^d and the two-impurities Green's function is represented by $G_{ij,s}^d$ with i and j being the position of impurities. In the Lehmann representation, using eigenstates $|\alpha\rangle$ and eigenenergies E_α obtained from numerical calculations, these Green's functions are given by

$$G_s^d = \frac{1}{Z}\sum_{\alpha\alpha'} |\langle\alpha|d_s|\alpha'\rangle|^2 \frac{e^{-\beta E_\alpha} + e^{-\beta E_{\alpha'}}}{E - (E_{\alpha'} - E_\alpha) + i\delta},$$
$$G_{ij,s}^d = \frac{1}{Z}\sum_{\alpha\alpha'} \langle\alpha|d_{is}|\alpha'\rangle\langle\alpha'|d_{js}^\dagger|\alpha\rangle \frac{e^{-\beta E_\alpha} + e^{-\beta E_{\alpha'}}}{E - (E_{\alpha'} - E_\alpha) + i\delta}. \quad (55)$$

Clearly, additional peak structures are seen in σ_{xx} and $\Delta\sigma_{xy}$ shown in Fig. 9. The main peak right at the Landau level is due to the resonant scattering of conduction electrons in phase with screened impurities, while side peaks are located at the phase boundaries when extra density of states is released from the total screened state to partial screened or unscreened states. For instance, side peaks in Fig. 9(c) are due to the density of state released from the screened state to unscreened state for one Kondo impurity. These peaks are important experimental signatures for phases of Kondo impurities in strong magnetic fields.

In summary, we have generalized the iterative diagonalization procedure adopted in NRG to investigate Kondo impurities screened by discrete Landau levels. We find that the ground state generally oscillates in Kondo screened state, partially screened, and unscreened spin states. This leads to quantum oscillations observed in magnetization and conductivity of the system. In particular, we find peak structures in longitudinal conductivity that reflect changes of Kondo screening phases and are important features to be observed in experiments. While we have been focusing on one and two Kondo impurities, our results are applicable to systems with a finite density of Kondo impurities. Our results thus provide a complete characterization of phases for Kondo effect in strong magnetic fields.

ACKNOWLEDGMENTS

This work was supported by National Science and Technology Council (NSTC), Taiwan. We also acknowledge support from Center for Quantum Technology within the framework of the Higher Education Sprout Project by the Ministry of Education (MOE) in Taiwan.

[1] A. C. Hewson, *The Kondo Problem to Heavy Fermions* (Cambridge University Press, Cambridge, England, 1993).

[2] P.-H. Chou, L.-J. Zhai, C.-H. Chung, C.-Y. Mou, and T.-K. Lee, Phys. Rev. Lett. **116**, 177002 (2016).

[3] S. Doniach, in *Valence Instabilities and Related Narrow Band Phenomena*, edited by R. D. Parks (Plenum, New York, 1977), p. 169; Physica B+C **91**, 231 (1977).
[4] J. R. Iglesias, C. Lacroix, and B. Coqblin, Phys. Rev. B **56**, 11820 (1997).
[5] C. Jayaprakash, H. R. Krishna-murthy, and J. W. Wilkins, Phys. Rev. Lett. **47**, 737 (1981).
[6] B. A. Jones and C. M. Varma, Phys. Rev. Lett. **58**, 843 (1987).
[7] B. A. Jones, C. M. Varma, and J. W. Wilkins, Phys. Rev. Lett. **61**, 125 (1988).
[8] B. A. Jones and C. M. Varma, Phys. Rev. B **40**, 324 (1989).
[9] J. B. Silva, W. L. C. Lima, W. C. Oliveira, J. L. N. Mello, L. N. Oliveira, and J. W. Wilkins, Phys. Rev. Lett. **76**, 275 (1996).
[10] P. Simon, R. Lopez, and Y. Oreg, Phys. Rev. Lett. **94**, 086602 (2005).
[11] T. Jabben, N. Grewe, and S. Schmitt, Phys. Rev. B **85**, 045133 (2012).
[12] A. Spinelli, M. Gerrits, R. Toskovic, B. Bryant, M. Ternes, and A. F. Otte, Nat. Commun. **6**, 10046 (2015).
[13] G. Li, Z. Xiang, F. Yu, T. Asaba, B. Lawson, P. Cai, C. Tinsman, A. Berkley, S. Wolgast, Y. S. Eo, D.-J. Kim, C. Kurdak, J. W. Allen, K. Sun, X. H. Chen, Y. Y. Wang, Z. Fisk, and L. Li, Science **346**, 1208 (2014).
[14] B. S. Tan, Y.-T. Hsu, B. Zeng, M. Ciomaga Hatnean, N. Harrison, Z. Zhu, M. Hartstein, M. Kiourlappou, A. Srivastava, M. D. Johannes, T. P. Murphy, J.-H. Park, L. Balicas, G. G. Lonzarich, G. Balakrishnan, and Suchitra E. Sebastian, Science **349**, 287 (2015).
[15] H. Liu, M. Hartstein, G. J. Wallace, A. J. Davies, M. C. Hatnean, M. D. Johannes, N. Shitsevalova, G. Balakrishnan, and S. E. Sebastian, J. Phys.: Condens. Matter **30**, 16LT01 (2018).
[16] Y.-W. Lu, P.-H. Chou, C.-H. Chung, T.-K. Lee, and C.-Y. Mou, Phys. Rev. B **101**, 115102 (2020).
[17] C. C. Yu and M. Guerrero, Phys. Rev. B **54**, 8556 (1996).
[18] K. Chen and C. Jayaprakash, Phys. Rev. B **57**, 5225 (1998).
[19] M. R. Galpin and D. E. Logan, Phys. Rev. B **77**, 195108 (2008).
[20] B. Dóra and P. Thalmeier, Phys. Rev. B **76**, 115435 (2007).
[21] M. A. Ruderman and C. Kittel, Phys. Rev. **96**, 99 (1954).
[22] T. Kasuya, Prog. Theor. Phys. **16**, 45 (1956).
[23] K. Yosida, Phys. Rev. **106**, 893 (1957).
[24] R. Bulla, T. A. Costi, and T. Pruschke, Rev. Mod. Phys. **80**, 395 (2008).
[25] J. Cao, H. A. Fertig, and S. Zhang, Phys. Rev. B **99**, 205430 (2019).
[26] See Supplemental Material at http://link.aps.org/supplemental/10.1103/PhysRevB.106.195107 for details of the calculation.
[27] H. R. Krishna-murthy, J. W. Wilkins, and K. G. Wilson, Phys. Rev. B **21**, 1003 (1980).
[28] H. R. Krishna-murthy, J. W. Wilkins, and K. G. Wilson, Phys. Rev. B **21**, 1044 (1980).
[29] T. A. Costi, Phys. Rev. Lett. **85**, 1504 (2000).
[30] J. Knolle and N. R. Cooper, Phys. Rev. Lett. **115**, 146401 (2015).
[31] T. Ando, Y. Matsumoto, and Y. Uemura, J. Phys. Soc. Jpn. **39**, 279 (1975).

Correction: In the front matter, the affiliation indicators for the second and third affiliations were not ascribed properly and have now been set right.